Revisiting western United States hydroclimate during the last deglaciation

Minmin Fu[1]

[1]Yale University

January 20, 2023

Abstract

During the last ice age, the western United States was covered by large lakes, sustained partly by higher levels of precipitation. Increased rainfall was driven by the atmospheric circulation associated with the presence of large North American ice sheets, yet Pleistocene lakes generally reached their highstands not at glacial maximum but during deglaciation. Prior modeling studies, however, showed nearly monotonic drying since the last glacial maximum. Here I show that iTraCE, a new transient climate simulation of the last deglaciation, reproduces a robust peak in winter rainfall over the Great Basin near 16 ka. The simulated peak is driven by a transient strengthening and southward shift of the midlatitude jet. While meltwater forcing is an important driver of changes to the North Pacific Jet, changing orbital conditions and rising atmospheric CO_2 also shift the jet south and contribute to wetter conditions over the western US during deglaciation.

Revisiting western United States hydroclimate during the last deglaciation

Minmin Fu[1]

[1]Department of Earth and Planetary Sciences, Yale University, New Haven, CT, USA

Key Points:

- Geological evidence indicates many lakes over the western United States reached highstands during the last deglaciation.
- iTraCE, a transient simulation of the last deglaciation, shows wetter conditions at 16 ka than at 20 ka and compares well to proxy evidence.
- Orbital conditions, rising atmospheric CO_2, and meltwater flux all contribute to lake expansions inferred during Heinrich Stadial 1.

Corresponding author: Minmin Fu, `minmin.fu@yale.edu`

Abstract

During the last ice age, the western United States was covered by large lakes, sustained partly by higher levels of precipitation. Increased rainfall was driven by the atmospheric circulation associated with the presence of large North American ice sheets, yet Pleistocene lakes generally reached their highstands not at glacial maximum but during deglaciation. Prior modeling studies, however, showed nearly monotonic drying since the last glacial maximum. Here I show that iTraCE, a new transient climate simulation of the last deglaciation, reproduces a robust peak in winter rainfall over the Great Basin near 16 ka. The simulated peak is driven by a transient strengthening and southward shift of the midlatitude jet. While meltwater forcing is an important driver of changes to the North Pacific Jet, changing orbital conditions and rising atmospheric CO_2 also shift the jet south and contribute to wetter conditions over the western US during deglaciation.

Plain Language Summary

At the height of the last ice age, the western United States was covered by large lakes such as Lake Bonneville and Lake Lahontan that required more rainfall to be sustained. It is believed that the three to four kilometer thick North American ice sheet over Canada acted as an obstacle to the atmospheric flow, forcing storms to be deflected southward over the southwestern US and bringing more winter rain. While wet conditions during glacial maximum are attributable to the presence of a large ice sheet, why does geological evidence indicate that most lakes attained their maximum size not when the ice sheet was at it largest, but rather when the ice sheet was already melting? Here, I use climate simulations to show that other factors, such as changes to Earth's tilt and temperature, in conjunction with changes in ocean circulation, caused a temporary further increase in rainfall that explains lake expansions during the deglaciation.

1 Introduction

The hydrological cycle over the western United States has varied dramatically in past climates (Fu et al., 2022; Ibarra et al., 2018). During the Last Glacial Maximum (LGM; $\sim$ 20 ka), much of western North America was covered in large lakes, reflecting increased precipitation and reduced potential evapotranspiration (Hostetler & Benson, 1990; Ibarra et al., 2014; Tabor et al., 2021). The Great Basin, the largest closed watershed over North America, is arid in the modern climate, yet was characterized by expansive lakes such as Lake Lahontan and Lake Bonneville during the last glacial period (Broecker & Orr, 1958; Mifflin & Wheat, 1979; Reheis et al., 2014). Multiple lines of geological evidence suggest that much of the southwestern US was wetter during the LGM, albeit with a dipole structure characterized by more-arid-than-present conditions over northwestern North America (Oster et al., 2015).

Previous studies have sought to identify the mechanism by which more rainfall was supplied to the Great Basin during the LGM. One hypothesis is that the Cordilleran and Laurentide ice sheets acted as a topographic obstacle that split or diverted the jet stream, leading to a southward deflection of midlatitude storms (COHMAP Members, 1988; Kutzbach & Wright Jr, 1985; Lora et al., 2017; Manabe & Broccoli, 1985). Another study suggested high ice-sheet albedo could suppress the North American Monsoon and enhance westerlies south of the ice sheet (Bhattacharya et al., 2017); other suggestions include moisture transport from the south (Lyle et al., 2012) or a midlatitude waveguide leading to different patterns of variability (Lofverstrom, 2020). Yet another study showed that mechanical forcing alone may be insufficient and that atmosphere-ocean feedbacks may play a role as well (Amaya et al., 2022). Although the detailed mechanisms of the atmospheric response continue to be debated, the presence of the Cordilleran and Laurentide ice sheets led to a major reconfiguration of the hydrological cycle over the western United States with ice-sheet topography, albedo, and air-sea fluxes all playing a role.

Modeling studies generally reproduce wetter conditions over the western US during the LGM (Brady et al., 2013; Kageyama et al., 2021; Kutzbach & Wright Jr, 1985; Lora et al., 2017; Scheff et al., 2017). However, a more subtle feature of the hydrological cycle during the last glacial period is that lake highstands over the western US were generally achieved during the last *deglaciation*, and not during the LGM (Lyle et al., 2012). Over the Great Basin, lake highstands at most sites occurred around Heinrich Stadial 1 (HS1; ~18 to 14.7 ka; Munroe & Laabs, 2013b; Reheis et al., 2014). An older transient simulation of the last deglaciation (TraCE-21ka), however, showed near-monotonic drying over the western US following the LGM (Lora & Ibarra, 2019), whereas increased precipitation is necessary to explain inferred lake expansions (McGee et al., 2018). Figure 1 shows maximum lake extents during the last deglaciation as well as a compilation of various basins and their highstand ages.

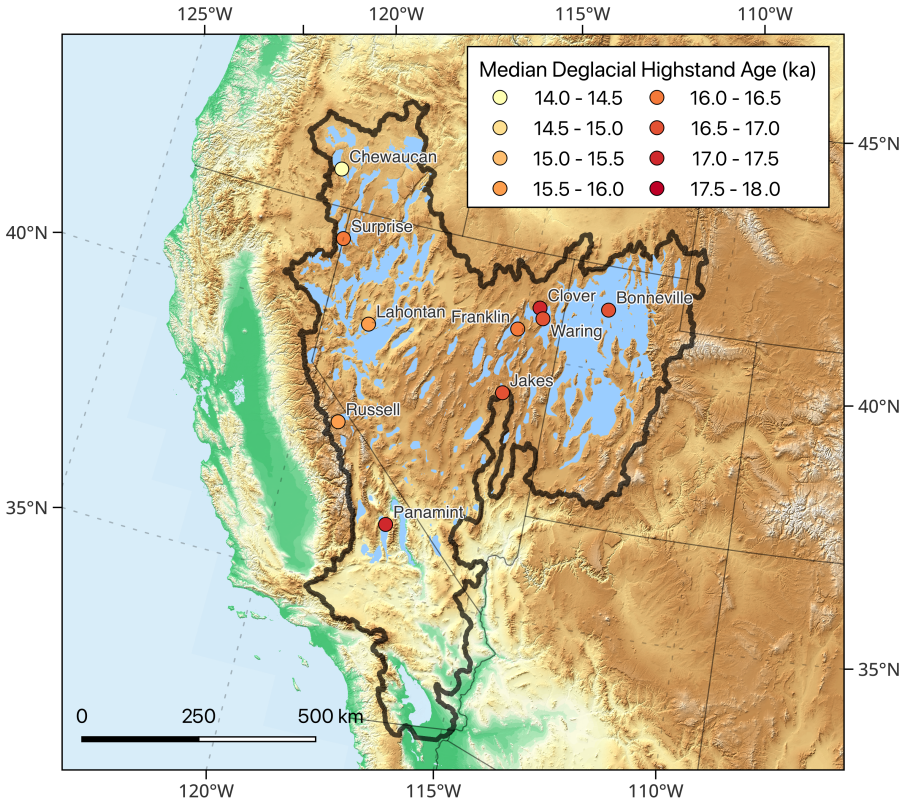

Figure 1. Topographic map of the western United States, showing the maximum extent of pluvial lakes during the last deglaciation (Mifflin & Wheat, 1979) and the median timing of deglacial highstands. The black curve outlines the Great Basin watershed boundary. Approximate age of deglacial lake highstands shown for Lake Bonneville (18–16 ka; McGee et al., 2012; Oviatt, 2015), Chewaucan Basin (14.2±0.2 to 14.6±0.3 ka; Hudson et al., 2017), Clover Basin (17.3±0.2 ka; Munroe & Laabs, 2013b), Franklin Basin (15.8±0.2 to 16.4±0.2 ka; Munroe & Laabs, 2013a), Lake Waring (16.6±0.4 ka; Munroe & Laabs, 2013b; García & Stokes, 2006), Jakes Basin (16.8±0.2 ka; García & Stokes, 2006), Lahontan Basin (15.7±0.2 ka; Adams & Wesnousky, 1998), Lake Russell (15.7±0.2 ka; Benson et al., 1998), Panamint Basin (17.0±0.3 to 17.2±0.3 ka; Jayko et al., 2008), and Surprise Basin (16 ka; Ibarra et al., 2014; Egger et al., 2018). Data compilation adapted from McGee et al. (2018) with Surprise Basin updated following Egger et al. (2018).

Here, I investigate the cause of western US lake expansions during the last deglaciation using the isotope-enabled transient climate experiment (iTraCE), a new transient simulation of the last deglaciation. iTraCE reproduces a robust peak in winter rainfall over the Great Basin at ∼16 ka. By utilizing the "stacked forcing" experiments offered by iTraCE, where four major forcing factors (ice sheet boundary conditions, insolation forcing, greenhouse gases, and meltwater fluxes) are applied additively, I quantify the contributions of these factors to the prominent peak in rainfall seen at ∼16 ka. Finally, I compare iTraCE to the earlier TraCE-21ka simulation and suggest that TraCE-21ka may fail to simulate deglacial lake expansions in this region because it produces a LGM climate that is too wet.

In Section 2, I introduce my methodology, including details about the iTraCE and TraCE-21ka simulations and their boundary conditions. Section 3 describes my results, including analysis of the western US hydrological cycle, North Pacific atmospheric circulation, and their sensitivity to meltwater fluxes, insolation, atmospheric CO_2, and ice sheet retreat. I conclude and discuss implications of the results in Section 4.

2 Methods

This study utilizes iTraCE, a simulation of the last deglaciation from 20 to 11 ka. iTraCE is performed with the isotope enabled version of the Community Earth System Model version 1.3 (iCESM1.3; Brady et al., 2019) and compares favorably to Greenland ice core oxygen isotope $\delta^{18}O$ records (He et al., 2021a) and speleothem records of Asian monsoon rainfall (He et al., 2021b). Key differences between TraCE-21ka (an older simulation also used in this study; Liu et al., 2009) and iTraCE include a model update from CCSM3 to iCESM1.3, whereby the atmospheric component changed from the Community Atmosphere Model version 3 (CAM3) to version 5.3 (iCAM5.3). Additionally, ice sheet boundary conditions were updated from ICE-5G (Peltier, 2004) to ICE-6G (Peltier et al., 2015), and iTraCE is run at ∼2° horizontal resolution rather than the 3.75° resolution of TraCE-21ka. Ice sheet topography (Peltier et al., 2015) and deglacial CO_2 (Lüthi et al., 2008; Monnin et al., 2001) are shown in Supplementary Information Figs. S1,S2.

To allow for the separation of individual forcing factors, iTraCE includes simulations with major forcing factors applied additively. Starting with LGM (20 ka) conditions, the (ICE) experiment involves evolving only ice sheets and ocean bathymetry. Next, insolation forcing from changing orbital conditions was added (ICE+ORB). Then, greenhouse gases and (ICE+ORB+GHG) and meltwater fluxes were applied (ICE+ORB+GHG+MWF). This allows for approximate decomposition of the role of individual forcing factors through differencing pairs of experiments. I will refer to the first three experiments as ICE, ICE+ORB, and ICE+ORB+GHG; the experiment with all four forcing factors (ICE+ORB+GHG+MWF) will simply be referred to as iTraCE.

I also utilize a fully coupled CESM1.2 simulation as a preindustrial reference. Differences between CESM1.3 and CESM1.2 are minor, and involve a different gravity wave scheme and a few bug fixes in the radiative scheme (Meehl et al., 2019). CESM1.3 produces a preindustrial climate similar to CESM1.2 (Hurrell et al., 2013), so the preindindustrial CESM1.2 climate serves as a suitable control simulation. For comparison to reanalysis, I use monthly-averaged precipitation and evaporation fields from ERA5 (Hersbach et al., 2020) over the period of 1979 to 2019. Monthly-averaged data from iTraCE and TraCE-21ka are used, and figures of specific ages show the climatology of a 500-year window centered on the relevant time period (e.g., 18 ka conditions are defined as the 18.25–17.75 ka climatology).

3 Results

CESM1.2 reproduces preindustrial precipitation minus evaporation ($P - E$) patterns in reasonable agreement with ERA5 reanalysis over western North America (Fig. S3), and iTraCE produces wetter-than-preindustrial conditions during the LGM (Fig. 2b). iTraCE shows a small decrease in $P - E$ compared to LGM over the western US at 18 ka (Fig. 2c), followed by a large increase at 16 ka along much of the California coast (Fig. 2d). Most of the western US is drier than at LGM at 14 ka (Fig. 2e), with a return to near-LGM conditions at 12 ka (Fig. 2f). The same figure, for TraCE-21ka, is shown in Fig. S4.

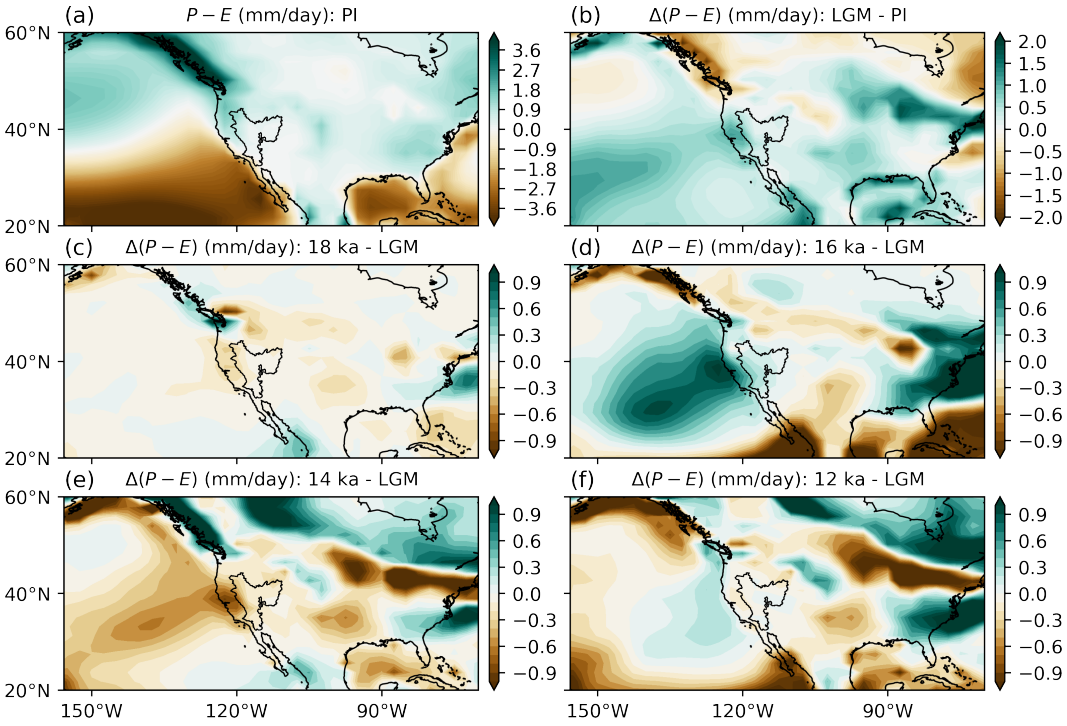

Figure 2. Maps of annual-mean $P - E$ in iTraCE. (a) $P - E$ in the preindustrial simulation. (b) Difference in $P - E$ between LGM (20 ka) and PI. (c) Difference between 18 ka and LGM. (d–f) As in (c), but for differences between 16, 14, and 12 ka from LGM respectively.

Figure 3 shows timeseries of annual-mean P and $P - E$ averaged over the Great Basin watershed. Precipitation decreases modestly from LGM to 18 ka, the start of Heinrich Stadial 1 (HS1; 18–14.7 ka). Precipitation then increases during HS1 until reaching a deglacial maximum around 16 ka that persists until 15 ka, the beginning of the Bølling-Allerød (14.7–13 ka). A rapid transition to dryer conditions is seen between 15 and 14 ka, while a modest increase in P and $P - E$ is seen during the Younger Dryas (13–11.5 ka). Whereas TraCE-21ka shares some features with iTraCE, such as rapid drying of the southwestern US during the Bølling-Allerød, the prominent peak in rainfall during HS1 is almost totally absent in TraCE-21ka (gray curve). Fig. S5 shows the hydrological cycle in iTraCE for individual seasons and shows that changes in annual-mean P and $P - E$ are dominated by changes in winter rainfall.

Rainfall over the western US during the LGM is dominated by winter rain, and occurs in association with midlatitude cyclones and atmospheric rivers (Lora et al., 2017). The position and trajectories of storms are strongly influenced by the position of the midlatitude jet, and it is therefore useful to diagnose changes in the North Pacific jet (NPJ) over the course of deglaciation. I find that the LGM state from iTraCE results in a south-

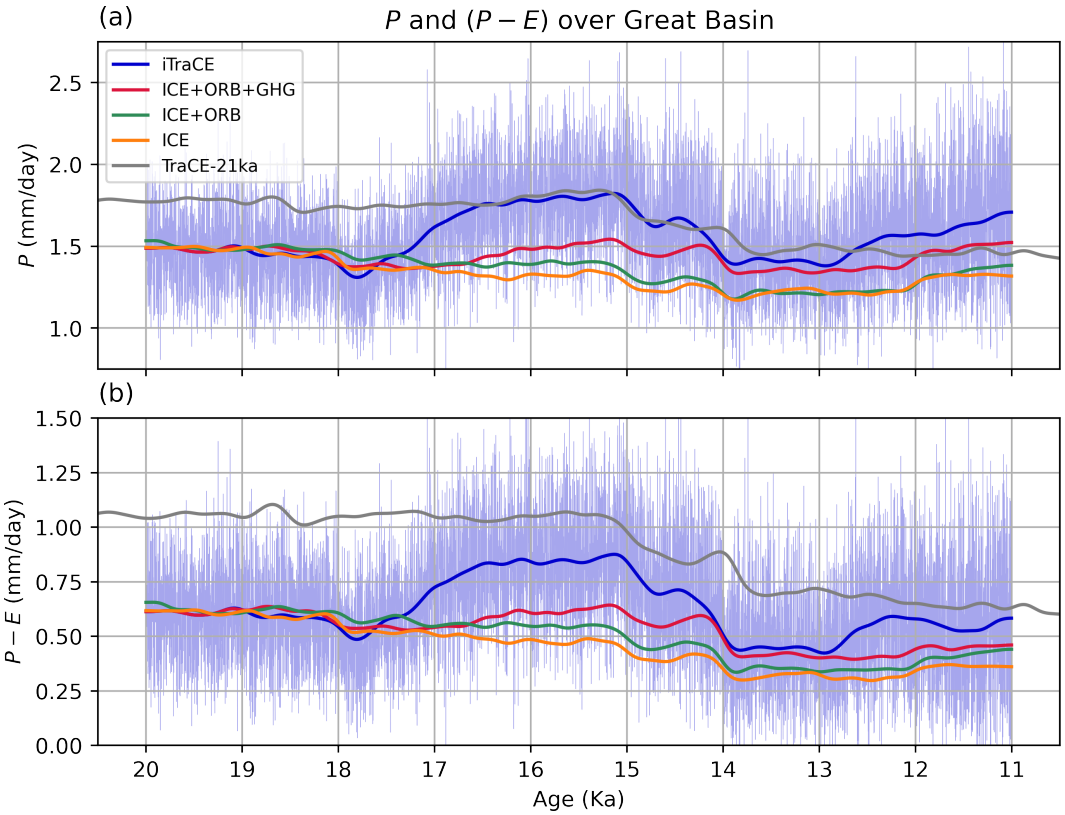

Figure 3. Hydrological cycle during deglaciation, averaged over the Great Basin watershed for experiments with four major forcing factors applied additively. (a) Annual-mean precipitation (P) from iTraCE, from 20 ka to 11 ka shown in the thin blue curve. The solid curves show the long term trend for all experiments, with a Gaussian filter ($\sigma = 100$) applied. (b) As in panel (a), but for precipitation minus evaporation ($P - E$).

ward shift of the midlatitude jet compared to preindustrial, as shown by the difference in DJF zonal velocity at 500 hPa (U500) between LGM and PI (Fig. 4b). This southward shift has recently been attributed to a PDO-like SST pattern induced by a stationary wave response to ice-sheets that is amplified by low cloud feedbacks over the North Pacific (Amaya et al., 2022).

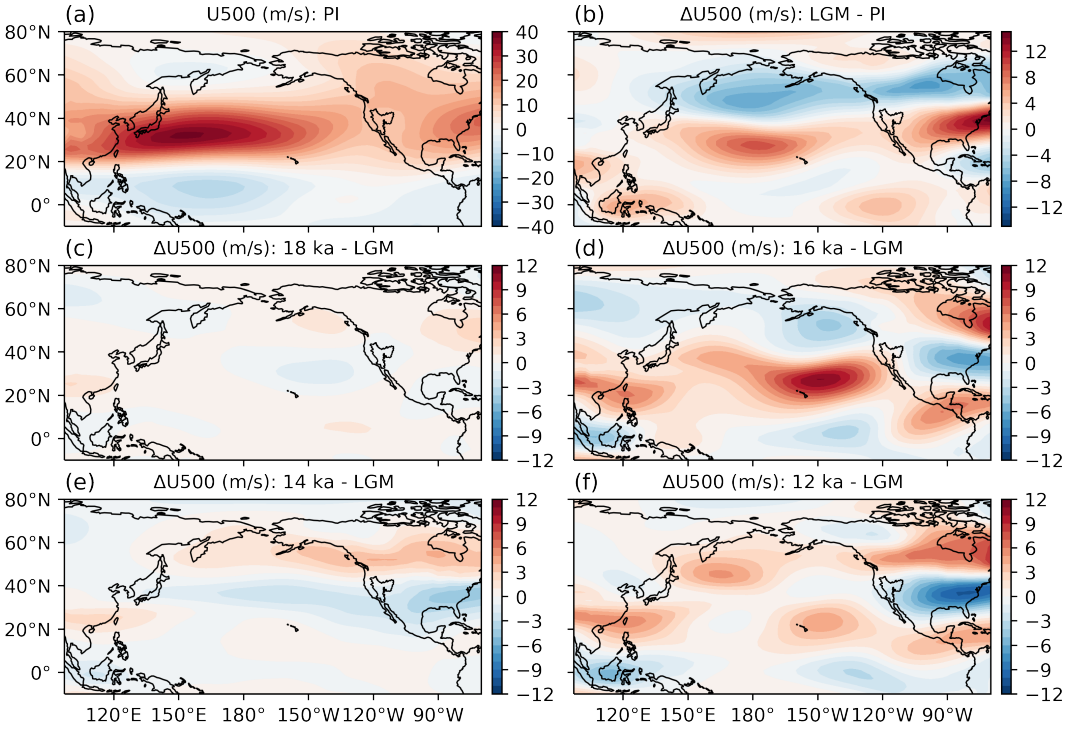

Figure 4. Winter-mean (DJF) atmospheric circulation over the North Pacific in iTraCE. (a) Zonal velocity at 500 hPa (U500; m/s) in the preindustrial simulation. (b) Difference in U500 between LGM (20 ka) and PI. (c) Difference between 18 ka and LGM. (d–f) As in (c), but for differences between 16, 14, and 12 ka from LGM respectively.

At 18 ka, a slight northward shift of the NPJ is seen compared to LGM, with weakening zonal winds south of 40 °N and strengthening winds to the north (Fig. 4c). However, at 16 ka, a dramatic intensification and southward shift occurs, leading to increased winter rainfall associated with the position of extratropical storms (Fig. 4d). At 14 ka, the NPJ again migrates northwards, consistent with rapid drying of southwestern North America seen during the Bølling-Allerød (Fig. 4e). Differences between 12 ka conditions and LGM are more ambiguous, with some acceleration seen both both the subtropical and sub-polar latitudes over the North Pacific basin (Fig. 4f). The same figure, for TraCE-21ka, is shown Fig. S6

I now examine the most prominent feature of the hydrological cycle over the southwestern US during the last deglaciation: the inference of lake expansions and generally wetter conditions during HS1. Given that iTraCE reproduces wetter conditions at HS1 that compare favorably to proxy evidence, I quantify the contribution of various forcing factors. As mentioned previously, iTraCE uses a "stacked forcing" approach that adds major forcing agents additively. I plot the long term trend in P and $P - E$ in these experiments in Fig. 3. The large difference between the full simulation (iTraCE) and the simulation excluding meltwater forcing (ICE+ORB+GHG) indicates that meltwater forcing plays a principal role in explaining lake expansions, leading to an increase in $P - E$

on the order of 0.22 mm/day. This is consistent with the midlatitude response to a southward shift of the intertropical convergence zone (ITCZ) in response to meltwater forcing, suggested by several studies (e.g., Chiang et al., 2014; Hudson et al., 2019; McGee et al., 2018).

Closer examination of the ICE and ICE+ORB experiments reveals that the contributions of insolation and greenhouse gas forcing to western US lake expansions are non-negligible, leading to a combined contribution of 0.15 mm/day in $P - E$. In the absence of all major forcing factors besides waning ice sheets (ICE), drying occurs, as expected. The ICE+ORB+GHG experiment shows that orbital forcing and rising atmospheric CO_2 concentration lead to wetting of the western US that roughly cancels the drying from ice-sheet retreat. This suggests that meltwater forcing alone, in the absence of GHG and orbital forcing, may not have been sufficient to explain observed lake expansions during HS1. Timeseries for stacked forcing experiments for individual seasons are shown in Fig. S7.

Linear decomposition of the difference between 16 ka and LGM into individual forcing factors reveals that orbital changes, greenhouse gas forcing, and meltwater at 16 ka each lead to a southward shift of the NPJ and increased $P - E$ over the Great Basin. The four panels of Fig. 5 represent contributions from meltwater flux, greenhouse gases, changing orbital conditions, and changing ice sheet boundary conditions. Rising GHGs lead to a southward shift of the jet (Fig. 5b), in contrast to inferences of a poleward shift under future warming scenarios. The response of the midlatitude jet to GHG forcing is complex, involving competing influences of increasing stratification and weakening meridional SST gradients (Shaw et al., 2016); the equatorward shift seen here is not entirely unexpected given the different LGM mean state. Figure 5c shows that changing orbital conditions further shift the jet southward, whereas a poleward shift occurs when only ice changes between LGM and 16 ka (Fig. 5d). Maps of differences in $P - E$ linearly separated are shown in Fig. S8 and agree with Fig. 3; transects of DJF zonal winds averaged between 120°W and 150°W are shown in Fig. S9.

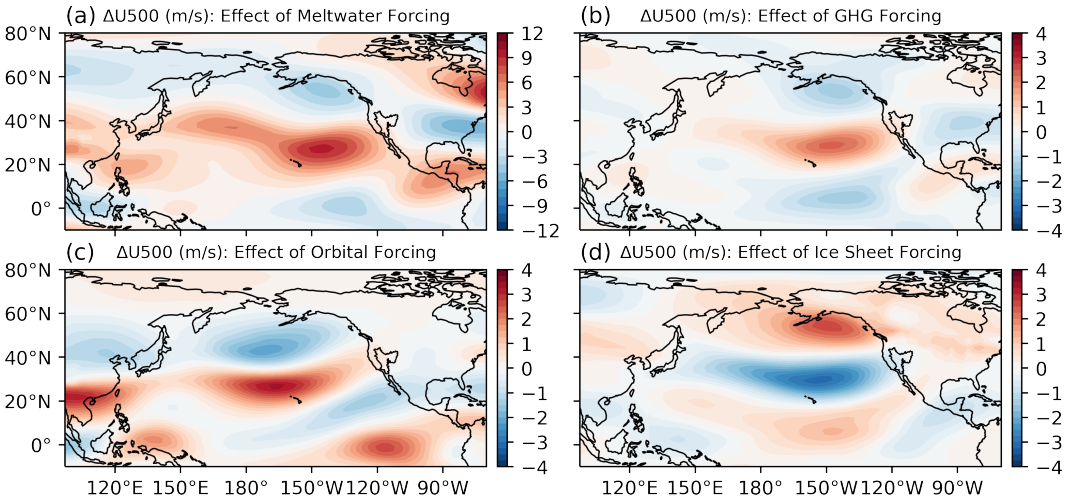

Figure 5. Difference in winter-mean (DJF) atmospheric circulation between 16 ka and LGM in iTraCE, decomposed into contributions from various forcing factors. (a) Difference in zonal velocity at 500 hPa (U500; m/s) from meltwater forcing (16 ka - 16 ka_ICE+ORB+GHG). (b) Effect of greenhouse gas forcing (16 ka_ICE+ORB+GHG - 16 ka_ICE+ORB). (c) Effect of orbital forcing (16 ka_ICE+ORB - 16 ka_ICE). (d) Effect of changing ice sheets and bathymetry (16 ka_ice - LGM).

Meridional temperature gradients modify the strength and position of the North Pacific jet through thermal wind balance, with orbital changes, greenhouse gas forcing, and meltwater forcing at HS1 each influencing the meridional temperature gradient over the North Pacific. As shown in Fig. S10b, 16 ka conditions are characterized by a southward shift of thermal equator, with cooling over most of the northern hemisphere and warming over North America and the southern hemisphere. This is primarily driven by North Atlantic meltwater fluxes, as seen in the contribution of this forcing factor (Fig. S10c). Closer examination of GHG forcing reveals a pattern of polar-amplified warming, a common feature of the surface temperature response to greenhouse gas forcing (Fig. S10d). This warming is particularly prominent in the North Atlantic as well as the the western North Pacific, as well as south of 50°S over the southern ocean.

Orbital forcing leads to modest cooling in the low latitudes but warming at high latitudes, particularly north of $\sim$ 40°N (Figs. 6,S10e). This can be understood primarily as a response to increasing orbital obliquity between 20 ka and 16 ka (Berger & Loutre, 1991). The LGM was characterized by a moderate axial tilt (23.13°), whereas 16 ka was characterized by a relatively high obliquity of 23.76°. This leads to increased insolation north of 45°N and reduced insolation equatorward of this latitude (Fig. S11), helping to explain the large-scale SST differences seen in Figs. 6,S10. A plot of differences in zonal-mean surface temperature between 16 ka and LGM is shown in Fig. 6. Meltwater forcing leads to a strengthening of meridional surface temperature gradients in the northern hemisphere midlatitudes, contributing to the intensification of the North Pacific jet seen during HS1 (Fig. 5a). Orbital and greenhouse gas forcing lead to strong polar amplified warming that reduces meridional SST gradients on the poleward flank of the NPJ, both contributing to a deceleration of the jet north of around 40 °N (Figs. 5b,c).

4 Discussion and Conclusions

In this study I used iTraCE, a transient simulation of the last deglaciation, to study deglacial hydroclimate over the western US. iTraCE simulates a 20% increase in annual mean rainfall and 38% increase in $P - E$ over the Great Basin from LGM to 16 ka that compares well to proxy evidence of HS1 lake expansions. Increased rainfall results principally from meltwater forcing, with changes in orbital forcing and GHG concentrations also playing a role. Wetter conditions during HS1 are associated with an intensification and southward shift of the North Pacific jet. After 15 ka, the North American ice sheets retreat rapidly and the jet shifts northwards towards its modern configuration.

The fact that iTraCE simulates climate changes over the western US in agreement with various proxy records is encouraging. A southward shift of the thermal equator during Heinrich Stadials is supported by high-resolution Antarctic methane records (Rhodes et al., 2015), East Asian speleothem δ^{18}O records (Wang et al., 2001), and sedimentary records from off the coast of Venezuela (Deplazes et al., 2013). The resulting response of the North Pacific jet has also been described (e.g., Broecker & Putnam, 2013; Chiang et al., 2014; Hudson et al., 2019), with McGee et al. (2018) showing that the NPJ response directly relates to the degree of southward shift of the central Pacific ITCZ. Yet this study, for the first time, has identified the imprint of these large-scale wind and SST changes on the deglacial hydrological cycle of the western US in a simulation with realistic boundary conditions.

While the 38% increase in $P - E$ that I identified falls short of fully explaining the magnitude of lake expansions during the last deglaciation, which ranged from 49% to 82% compared to LGM (McGee et al., 2018), it represents a notable improvement over previous modeling studies. It is possible that lake and vegetation feedbacks (e.g., Hostetler et al., 1994), absent in iTraCE due to the prescribed nature of land types, or an increase in runoff ratio with increasing basin-wide $P - E$ (Broecker, 2010), may further amplify the HS1 signal I identified. It is also possible that small misalignments of large-scale $P - E$

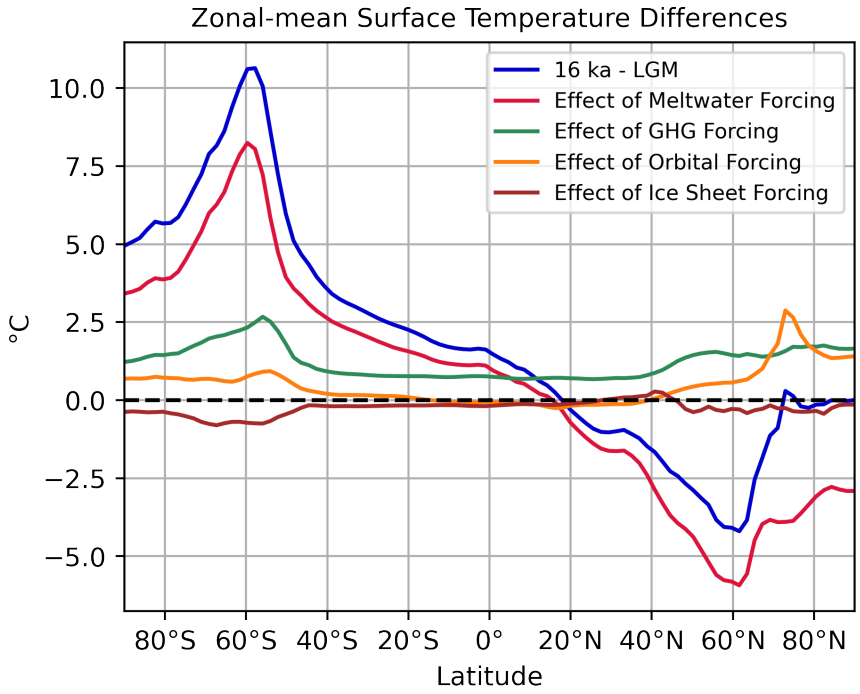

Figure 6. Zonal-mean and annual-mean surface temperature differences between 16 ka and LGM. The blue curve is the full difference between 16 ka and LGM, the red curve isolates the effect of meltwater forcing by subtracting the (16 ka_ICE+ORB+GHG) from the full 16 ka simulation, the green curve isolates GHG forcing (16 ka_ICE+ORB+GHG - 16 ka_ICE+ORB), the orange curve isolates orbital forcing (16 ka_ICE+ORB - 16 ka_ICE), and the brown curve isolates the ice sheet forcing (16 ka_ICE - LGM).

patterns with the relatively small Great Basin domain could explain why they do not perfectly match proxy records. For instance, $P - E$ increases at HS1 are largest along the coast; small horizontal offsets could change the inferred signal.

One caveat of the approach employed in this study is that the decomposition of the forced responses works insofar as they can be considered linear forcings. McGee et al. (2018) presented idealized hosing experiments in a low resolution climate model, with ice sheets fixed at LGM conditions and obliquity/precession set to extreme values to explore maximum/minimum possible northern hemisphere seasonality. They showed that the climate response to hosing under varied orbital conditions could be quite different, so if the forcing factors in iTraCE were applied in a different order, the decompositions shown here could also change. Therefore, the precise magnitude of the contributions of meltwater forcing, orbit, and greenhouse gases shown in this study should ultimately be taken as approximate.

This study also sheds light on why TraCE-21ka, an earlier transient simulation, did not reproduce wetter conditions at HS1 compared to LGM. One plausible explanation is that the ICE-5G reconstruction, which is too thick in the central sector of the Laurentide Ice Sheet (Argus & Peltier, 2010), may lead to an anomalously strong southward shift of the NPJ (as seen in Fig. S6b), and a TraCE-21ka LGM climate that is too wet (Fig. S4b). Indeed, Fig. 3 shows much higher P and $P - E$ in TraCE-21ka compared to iTraCE prior to HS1, with better agreement during HS1 and afterwards. Furthermore, comparison of 16ka winds and $P - E$ with PI (rather than LGM) conditions for both iTraCE and TraCE-21ka (Fig. S12) reveals patterns and amplitudes in agreement with each other, whereas these two simulations simulate considerably different LGM climates (Figs. 2b,4b,S4b,S6b).

While these diagnostics seem to suggest that revised ice sheet boundary conditions may explain iTraCE's improved simulation of western US climate during deglaciation, the impact of model version and increased horizontal resolution cannot yet be ruled out. Differences between iTraCE and TraCE-21ka should therefore be examined more closely in future studies, as this may provide insight on the robustness of these models for simulating future changes over the western US, a region whose future atmospheric circulation and hydrology are marked by great model uncertainty (Cvijanovic et al., 2017; Simpson et al., 2014; Seager et al., 2014).

Open Research

All post-processing scripts are available at `https://doi.org/10.5281/zenodo.7554840`. iTraCE output is available from `https://doi.org/10.26024/b290-an76` and TraCE-21ka output is available from `https://www.earthsystemgrid.org/project/trace.html`.

Acknowledgments

I thank Peter Molnar, Eli Tziperman, Jerry Mitrovica, Jiang Zhu, Tamara Pico, and Dan Ibarra for discussions. I thank Bette Otto-Bliesner, Esther Brady, Robert Tomas, Zhengyu Liu, and Chengfei He, who produced iTraCE. This research was supported by the NSF Climate Dynamics program (joint NSF/NERC) grant AGS-1924538 and the Flint Postdoctoral Fellowship at Yale. I would like to acknowledge high-performance computing support from Cheyenne (doi:10.5065/D6RX99HX) provided by NCAR's Computational and Information Systems Laboratory, sponsored by the National Science Foundation. I thank editor Sarah Feakins and four anonymous reviewers for helpful comments.

References

Adams, K. D., & Wesnousky, S. G. (1998). Shoreline processes and the age of the

Lake Lahontan highstand in the Jessup embayment, Nevada. *Geological Society of America Bulletin*, *110*(10), 1318–1332.

Amaya, D. J., Seltzer, A. M., Karnauskas, K. B., Lora, J. M., Zhang, X., & DiNezio, P. N. (2022). Air-sea coupling shapes North American hydroclimate response to ice sheets during the Last Glacial Maximum. *Earth and Planetary Science Letters*, *578*, 117271.

Argus, D. F., & Peltier, W. R. (2010). Constraining models of postglacial rebound using space geodesy: a detailed assessment of model ICE-5G (VM2) and its relatives. *Geophysical Journal International*, *181*(2), 697–723.

Benson, L. V., Lund, S. P., Burdett, J. W., Kashgarian, M., Rose, T. P., Smoot, J. P., & Schwartz, M. (1998). Correlation of late-Pleistocene lake-level oscillations in Mono Lake, California, with North Atlantic climate events. *Quaternary Research*, *49*(1), 1–10.

Berger, A., & Loutre, M. F. (1991). Insolation values for the climate of the last 10 million years. *Quat. Sci. Rev.*, *10*, 297-317.

Bhattacharya, T., Tierney, J. E., & DiNezio, P. (2017). Glacial reduction of the North American Monsoon via surface cooling and atmospheric ventilation. *Geophysical Research Letters*, *44*(10), 5113–5122.

Brady, E. C., Otto-Bliesner, B. L., Kay, J. E., & Rosenbloom, N. (2013). Sensitivity to glacial forcing in the CCSM4. *Journal of Climate*, *26*(6), 1901–1925.

Brady, E. C., Stevenson, S., Bailey, D., Liu, Z., Noone, D., Nusbaumer, J., ... others (2019). The connected isotopic water cycle in the community earth system model version 1. *Journal of Advances in Modeling Earth Systems*, *11*(8), 2547–2566.

Broecker, W. S. (2010). Long-term water prospects in the western United States. *Journal of Climate*, *23*(24), 6669–6683.

Broecker, W. S., & Orr, P. C. (1958). Radiocarbon chronology of Lake Lahontan and Lake Bonneville. *Geological Society of America Bulletin*, *69*(8), 1009–1032.

Broecker, W. S., & Putnam, A. E. (2013). Hydrologic impacts of past shifts of Earth's thermal equator offer insight into those to be produced by fossil fuel CO2. *Proceedings of the National Academy of Sciences*, *110*(42), 16710–16715.

Chiang, J. C. H., Lee, S.-Y., Putnam, A. E., & Wang, X. (2014). South pacific split jet, ITCZ shifts, and atmospheric north–south linkages during abrupt climate changes of the last glacial period. *Earth and Planetary Science Letters*, *406*, 233–246.

COHMAP Members. (1988). Climatic changes of the last 18,000 years: observations and model simulations. *Science*, *241*(4869), 1043–1052.

Cvijanovic, I., Santer, B. D., Bonfils, C., Lucas, D. D., Chiang, J. C., & Zimmerman, S. (2017). Future loss of Arctic sea-ice cover could drive a substantial decrease in California's rainfall. *Nature communications*, *8*(1), 1–10.

Deplazes, G., Lückge, A., Peterson, L. C., Timmermann, A., Hamann, Y., Hughen, K. A., ... others (2013). Links between tropical rainfall and North Atlantic climate during the last glacial period. *Nature Geoscience*, *6*(3), 213–217.

Egger, A. E., Ibarra, D. E., Weldon, R., Langridge, R. M., Marion, B., Hall, J., ... Rosen, M. R. (2018). Influence of pluvial lake cycles on earthquake recurrence in the northwestern Basin and Range, USA. *Geological Society of America Special Paper*, *536*, 1–28.

Fu, M., Cane, M. A., Molnar, P., & Tziperman, E. (2022). Warmer Pliocene upwelling site SST leads to wetter subtropical coastal areas: a positive feedback on SST. *Paleoceanography and Paleoclimatology*, *37*(2), e2021PA004357.

García, A. F., & Stokes, M. (2006). Late Pleistocene highstand and recession of a small, high-altitude pluvial lake, Jakes Valley, central Great Basin, USA. *Quaternary Research*, *65*(1), 179–186.

He, C., Liu, Z., Otto-Bliesner, B., Brady, E., Zhu, C., Tomas, R., ... others (2021b).

Hydroclimate footprint of pan-asian monsoon water isotope during the last deglaciation. *Science Advances*, *7*(4), eabe2611.

He, C., Liu, Z., Otto-Bliesner, B. L., Brady, E. C., Zhu, C., Tomas, R., ... Severinghaus, J. P. (2021a). Abrupt Heinrich Stadial 1 cooling missing in Greenland oxygen isotopes. *Science advances*, *7*(25), eabh1007.

Hersbach, H., Bell, B., Berrisford, P., Hirahara, S., Horányi, A., Muñoz-Sabater, J., ... others (2020). The ERA5 global reanalysis. *Quarterly Journal of the Royal Meteorological Society*, *146*(730), 1999–2049.

Hostetler, S. W., & Benson, L. V. (1990). Paleoclimatic implications of the high stand of Lake Lahontan derived from models of evaporation and lake level. *Climate dynamics*, *4*(3), 207–217.

Hostetler, S. W., Giorgi, F., Bates, G. T., & Bartlein, P. J. (1994). Lake-atmosphere feedbacks associated with paleolakes Bonneville and Lahontan. *Science*, *263*(5147), 665–668.

Hudson, A. M., Hatchett, B. J., Quade, J., Boyle, D. P., Bassett, S. D., Ali, G., & De los Santos, M. G. (2019). North-south dipole in winter hydroclimate in the western United States during the last deglaciation. *Scientific reports*, *9*(1), 1–12.

Hudson, A. M., Quade, J., Ali, G., Boyle, D., Bassett, S., Huntington, K. W., ... Wang, X. (2017). Stable C, O and clumped isotope systematics and ^{14}c geochronology of carbonates from the Quaternary Chewaucan closed-basin lake system, Great Basin, USA: Implications for paleoenvironmental reconstructions using carbonates. *Geochimica et Cosmochimica Acta*, *212*, 274–302.

Hurrell, J. W., Holland, M. M., Gent, P. R., Ghan, S., Kay, J. E., Kushner, P. J., ... others (2013). The community earth system model: a framework for collaborative research. *Bulletin of the American Meteorological Society*, *94*(9), 1339–1360.

Ibarra, D. E., Egger, A. E., Weaver, K. L., Harris, C. R., & Maher, K. (2014). Rise and fall of late Pleistocene pluvial lakes in response to reduced evaporation and precipitation: Evidence from Lake Surprise, California. *Bulletin*, *126*(11-12), 1387–1415.

Ibarra, D. E., Oster, J. L., Winnick, M. J., Caves Rugenstein, J. K., Byrne, M. P., & Chamberlain, C. P. (2018). Warm and cold wet states in the western United States during the Pliocene–Pleistocene. *Geology*, *46*(4), 355–358.

Jayko, A. S., Forester, R. M., Kaufman, D. S., Phillips, F. M., Yount, J. C., McGeehin, J., & Mahan, S. A. (2008). Late Pleistocene lakes and wetlands, Panamint Valley, Inyo County, California. *Late Cenozoic Drainage History of the Southwestern Great Basin and Lower Colorado River Region: Geologic and Biotic Perspectives,* edited by M.C. Reheis, R. Hershler, and D.M. Miller*, The Geological Society of America Special Paper 439*, 151-184.

Kageyama, M., Harrison, S. P., Kapsch, M.-L., Lofverstrom, M., Lora, J. M., Mikolajewicz, U., ... others (2021). The PMIP4 last glacial maximum experiments: preliminary results and comparison with the PMIP3 simulations. *Climate of the Past*, *17*(3), 1065–1089.

Kutzbach, J. E., & Wright Jr, H. E. (1985). Simulation of the climate of 18,000 years BP: Results for the North American/North Atlantic/European sector and comparison with the geologic record of North America. *Quaternary Science Reviews*, *4*(3), 147–187.

Liu, Z., Otto-Bliesner, B. L., He, F., Brady, E. C., Tomas, R., Clark, P. U., ... Cheng, J. (2009). Transient simulation of last deglaciation with a new mechanism for Bølling-Allerød warming. *Science*, *325*(5938), 310–314.

Lofverstrom, M. (2020). A dynamic link between high-intensity precipitation events in southwestern north america and europe at the last glacial maximum. *Earth and Planetary Science Letters*, *534*, 116081.

Lora, J. M., & Ibarra, D. E. (2019). The North American hydrologic cycle through

the last deglaciation. *Quaternary Science Reviews*, *226*, 105991.

Lora, J. M., Mitchell, J. L., Risi, C., & Tripati, A. E. (2017). North Pacific atmospheric rivers and their influence on western North America at the Last Glacial Maximum. *Geophysical Research Letters*, *44*(2), 1051–1059.

Lüthi, D., Le Floch, M., Bereiter, B., Blunier, T., Barnola, J.-M., Siegenthaler, U., ... others (2008). High-resolution carbon dioxide concentration record 650,000–800,000 years before present. *nature*, *453*(7193), 379–382.

Lyle, M., Heusser, L., Ravelo, C., Yamamoto, M., Barron, J., Diffenbaugh, N. S., ... Andreasen, D. (2012). Out of the tropics: the Pacific, Great Basin Lakes, and Late Pleistocene water cycle in the western United States. *Science*, *337*(6102), 1629–1633.

Manabe, S., & Broccoli, A. J. (1985). The influence of continental ice sheets on the climate of an ice age. *J. Geophys. Res.*, *90*, 2167–2190.

McGee, D., Moreno-Chamarro, E., Marshall, J., & Galbraith, E. (2018). Western US lake expansions during Heinrich stadials linked to Pacific Hadley circulation. *Science advances*, *4*(11), eaav0118.

McGee, D., Quade, J., Edwards, R. L., Broecker, W. S., Cheng, H., Reiners, P. W., & Evenson, N. (2012). Lacustrine cave carbonates: Novel archives of paleohydrologic change in the Bonneville Basin (Utah, USA). *Earth and Planetary Science Letters*, *351*, 182–194.

Meehl, G. A., Yang, D., Arblaster, J. M., Bates, S. C., Rosenbloom, N., Neale, R., ... others (2019). Effects of model resolution, physics, and coupling on southern hemisphere storm tracks in CESM1.3. *Geophysical Research Letters*, *46*(21), 12408–12416.

Mifflin, M. D., & Wheat, M. M. (1979). *Pluvial lakes and estimated pluvial climates of Nevada* (Vol. 94). Mackay School of Mines, University of Nevada.

Monnin, E., Indermuhle, A., Dallenbach, A., Fluckiger, J., Stauffer, B., Stocker, T. F., ... Barnola, J.-M. (2001). Atmospheric CO_2 concentrations over the last glacial termination. *science*, *291*(5501), 112–114.

Munroe, J. S., & Laabs, B. J. C. (2013a). Latest Pleistocene history of pluvial Lake Franklin, northeastern Nevada, USA. *GSA Bulletin*, *125*(3-4), 322–342.

Munroe, J. S., & Laabs, B. J. C. (2013b). Temporal correspondence between pluvial lake highstands in the southwestern US and Heinrich Event 1. *Journal of Quaternary Science*, *28*(1), 49–58.

Oster, J. L., Ibarra, D. E., Winnick, M. J., & Maher, K. (2015). Steering of westerly storms over western North America at the Last Glacial Maximum. *Nature Geoscience*, *8*(3), 201–205.

Oviatt, C. G. (2015). Chronology of Lake Bonneville, 30,000 to 10,000 yr BP. *Quaternary Science Reviews*, *110*, 166–171.

Peltier, W. R. (2004). Global glacial isostasy and the surface of the ice-age Earth: the ICE-5G (VM2) model and GRACE. *Annu. Rev. Earth Planet. Sci.*, *32*, 111–149.

Peltier, W. R., Argus, D., & Drummond, R. (2015). Space geodesy constrains ice age terminal deglaciation: The global ice-6g_c (vm5a) model. *Journal of Geophysical Research: Solid Earth*, *120*(1), 450–487.

Reheis, M. C., Adams, K. D., Oviatt, C. G., & Bacon, S. N. (2014). Pluvial lakes in the Great Basin of the western United States – A view from the outcrop. *Quaternary Science Reviews*, *97*, 33–57.

Rhodes, R. H., Brook, E. J., Chiang, J. C. H., Blunier, T., Maselli, O. J., McConnell, J. R., ... Severinghaus, J. P. (2015). Enhanced tropical methane production in response to iceberg discharge in the North Atlantic. *Science*, *348*(6238), 1016–1019.

Scheff, J., Seager, R., Liu, H., & Coats, S. (2017). Are glacials dry? Consequences for paleoclimatology and for greenhouse warming. *Journal of Climate*, *30*(17), 6593–6609.

Seager, R., Neelin, D., Simpson, I., Liu, H., Henderson, N., Shaw, T., ... Cook, B. (2014). Dynamical and thermodynamical causes of large-scale changes in the hydrological cycle over North America in response to global warming. *Journal of Climate*, *27*(20), 7921–7948.

Shaw, T., Baldwin, M., Barnes, E. A., Caballero, R., Garfinkel, C., Hwang, Y.-T., ... others (2016). Storm track processes and the opposing influences of climate change. *Nature Geoscience*, *9*(9), 656–664.

Simpson, I. R., Shaw, T. A., & Seager, R. (2014). A diagnosis of the seasonally and longitudinally varying midlatitude circulation response to global warming. *Journal of the Atmospheric Sciences*, *71*(7), 2489–2515.

Tabor, C., Lofverstrom, M., Oster, J., Wortham, B., de Wet, C., Montañez, I., ... Liu, Z. (2021). A mechanistic understanding of oxygen isotopic changes in the Western United States at the Last Glacial Maximum. *Quaternary Science Reviews*, *274*, 107255.

Wang, Y.-J., Cheng, H., Edwards, R. L., An, Z., Wu, J., Shen, C.-C., & Dorale, J. A. (2001). A high-resolution absolute-dated late Pleistocene monsoon record from Hulu Cave, China. *Science*, *294*(5550), 2345–2348.

Supporting Information for "Revisiting western United States hydroclimate during the last deglaciation"

Minmin Fu[1]

[1]Department of Earth and Planetary Sciences, Yale University, New Haven, CT, USA

Contents of this file

1. Figures S1 to S12

2. References

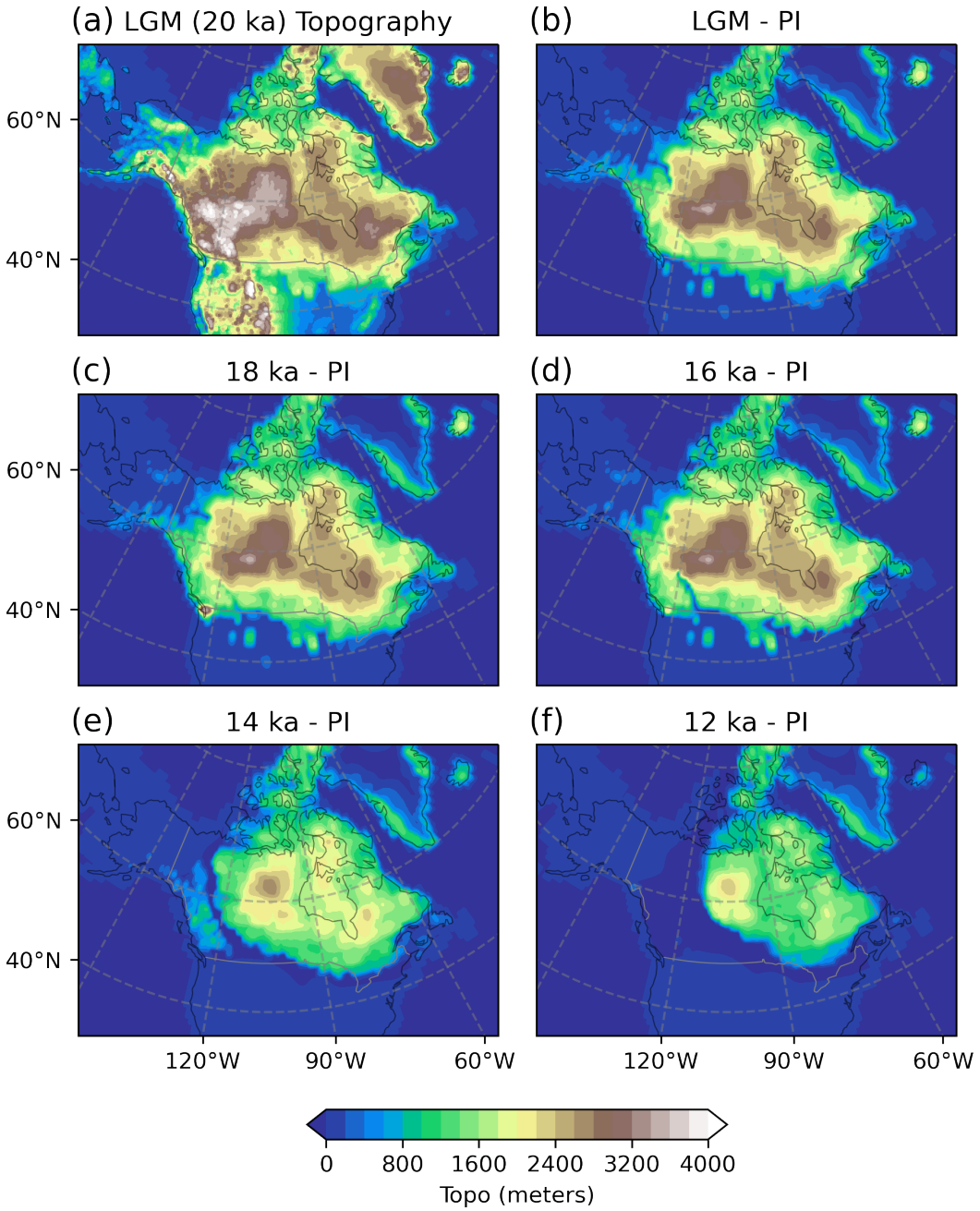

Figure S1. (a) Ice-sheet topography (meters) during the LGM (20 ka) from the ICE-6G reconstruction (Peltier et al., 2015). (b) Difference in ice-sheet topography between LGM and preindustrial. (c–f) As in (b), but differences from preindustrial for 18, 16, 14, and 12 ka, respectively.

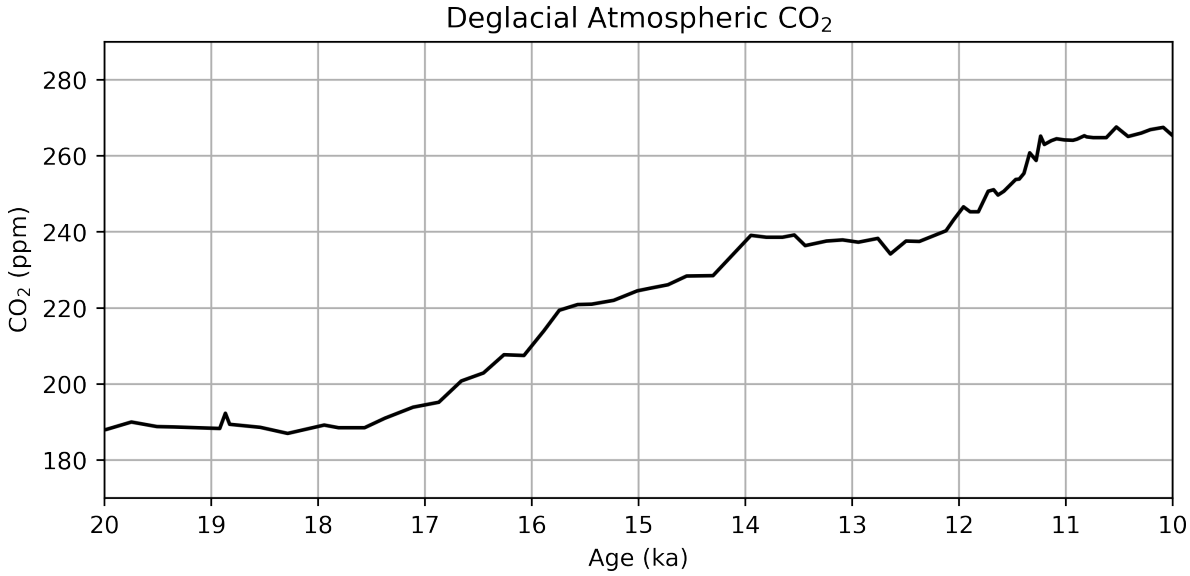

Figure S2. Atmospheric CO_2 concentration during the last deglaciation (Lüthi et al., 2008; Monnin et al., 2001).

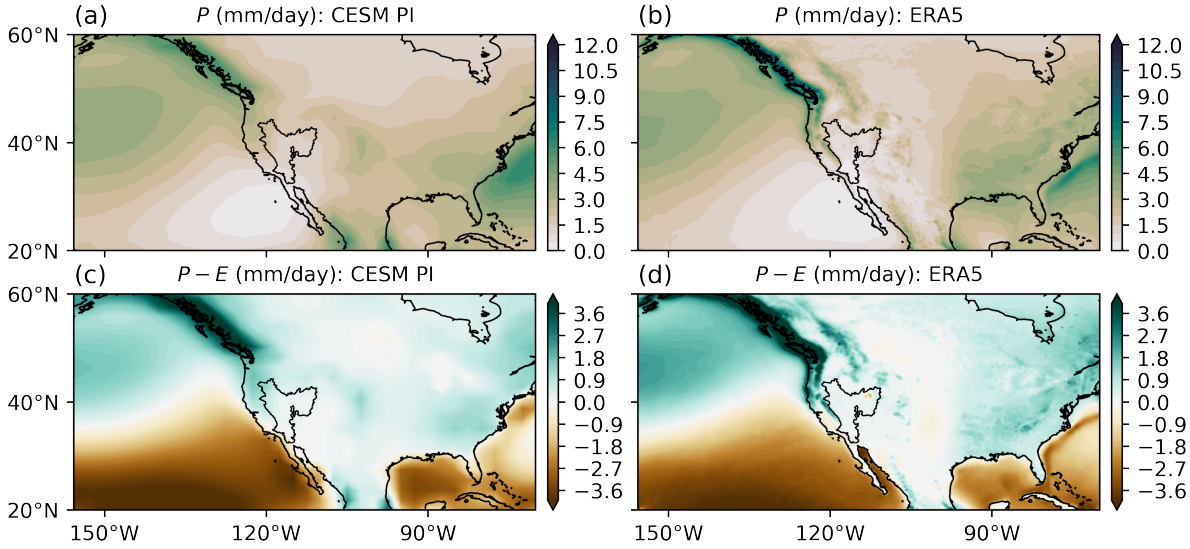

Figure S3. (a) Annual-mean precipitation rate for the preindustrial CESM 1.2 simulation. (b) As in (a), but for ERA5 reanalysis. (c) Annual-mean precipitation minus evaporation ($P - E$) for preindustrial CESM 1.2. (d) As in (c), but for ERA5 reanalysis.

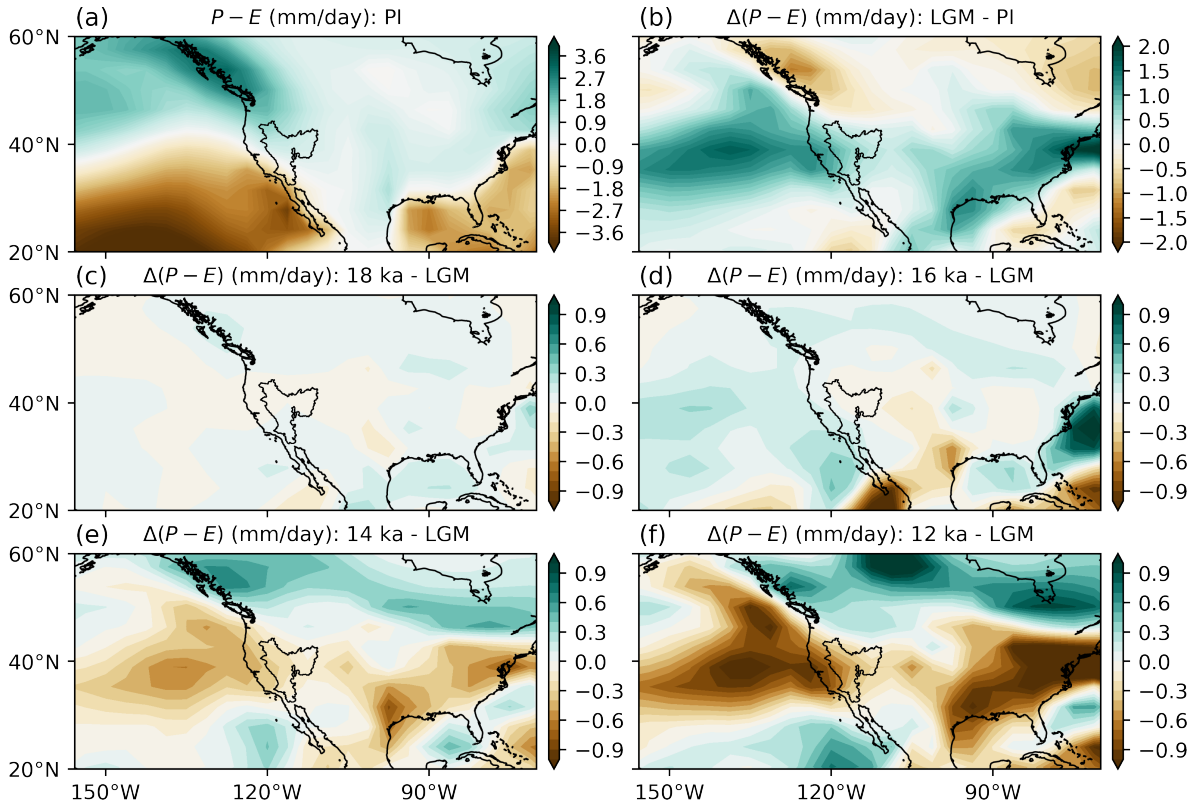

Figure S4. Maps of annual-mean $P-E$ in TraCE-21ka. (a) $P-E$ in the preindustrial simulation. (b) Difference in $P-E$ between LGM (20 ka) and PI. (c) Difference between 18 ka and LGM. (d–f) As in (c), but for differences between 16, 14, and 12 ka from LGM respectively.

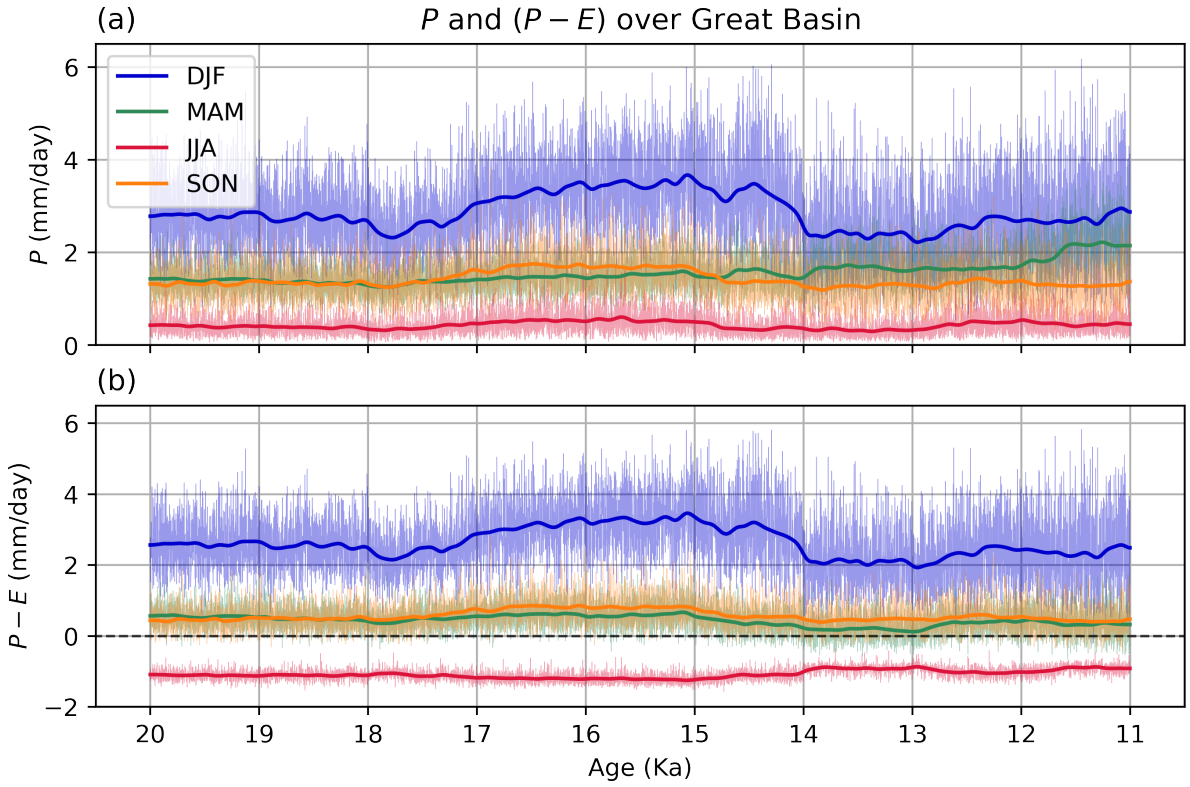

Figure S5. Hydrological cycle during deglaciation, averaged over the Great Basin watershed for individual seasons in iTraCE. (a) Seasonal mean precipitation (P), from 20 ka to 11 ka shown in the thin curve. The thick curve shows the long term trend, with a Gaussian filter ($\sigma = 100$) applied. (b) As in panel (a), but for precipitation minus evaporation ($P - E$).

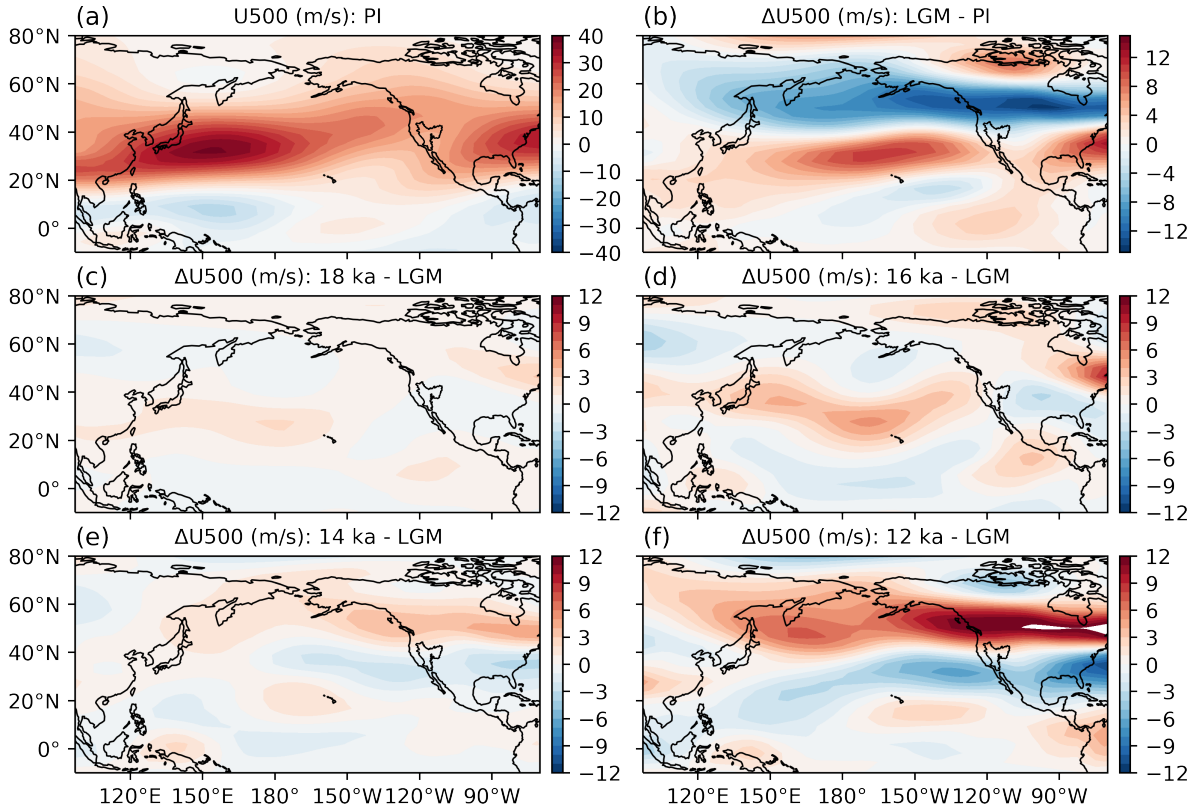

Figure S6. Winter-mean (DJF) atmospheric circulation over the North Pacific in TraCE-21ka. (a) Zonal velocity at 500 hPa (U500; m/s) in the preindustrial simulation. (b) Difference in U500 between LGM (20 ka) and PI. (c) Difference between 18 ka and LGM. (d–f) As in (c), but for differences between 16, 14, and 12 ka from LGM respectively.

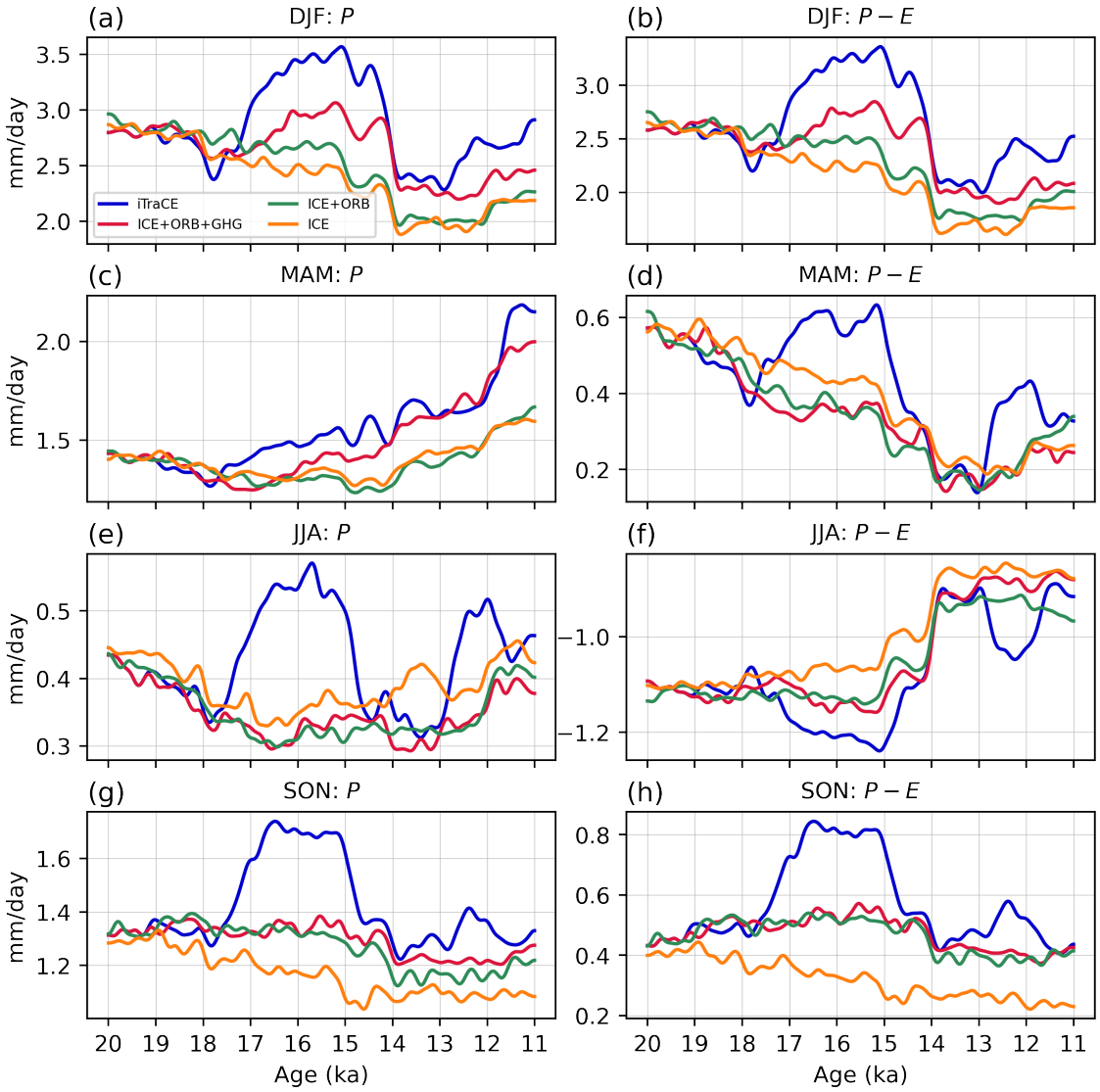

Figure S7. Hydrological cycle over the Great Basin watershed in additive forcing experiments, for individual seasons in iTraCE. (a) Long term trend in DJF-mean precipitation (P), from 20 ka to 11 ka, with four major forcing factors applied additively. A Gaussian filter ($\sigma = 100$) has been applied to all curves. (b) As in panel (a), but for precipitation minus evaporation ($P - E$). (c,d) As in (a,b), but for MAM. (e,f) As in (a,b), but for JJA. (g,h) As in (a,b), but for SON.

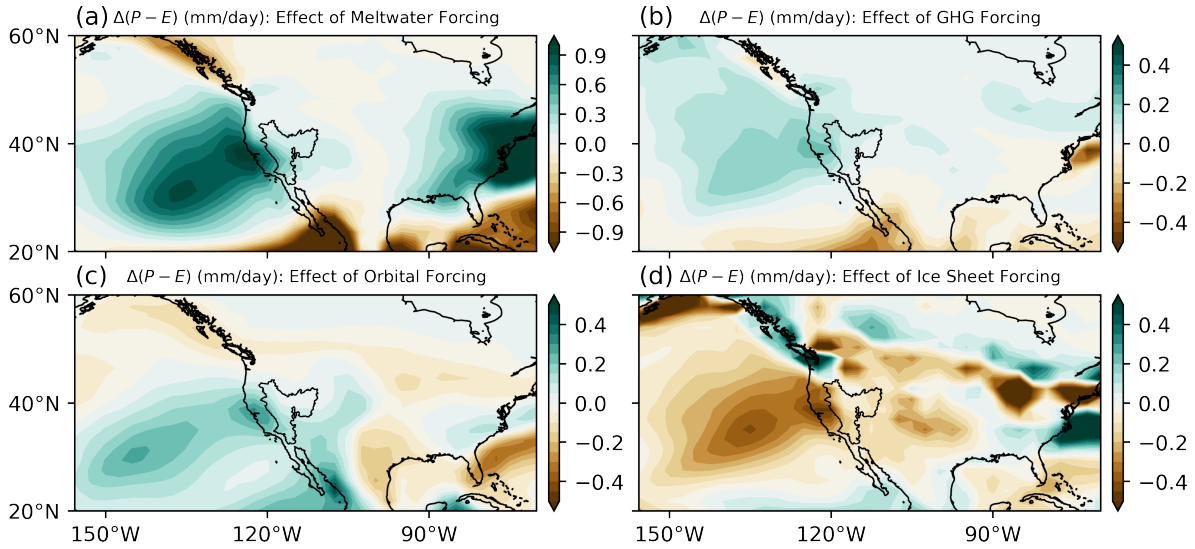

Figure S8. Difference in annual-mean $P - E$ between 16 ka and LGM in iTraCE, decomposed into contributions from various forcing factors. (a) Difference in $P - E$ from meltwater forcing (16 ka - 16 ka_ICE+ORB+GHG). (b) Effect of greenhouse gas forcing (16 ka_ICE+ORB+GHG - 16 ka_ICE+ORB). (c) Effect of orbital forcing (16 ka_ICE+ORB - 16 ka_ICE). (d) Effect of changing ice sheets and bathymetry (16 ka_ice - LGM).

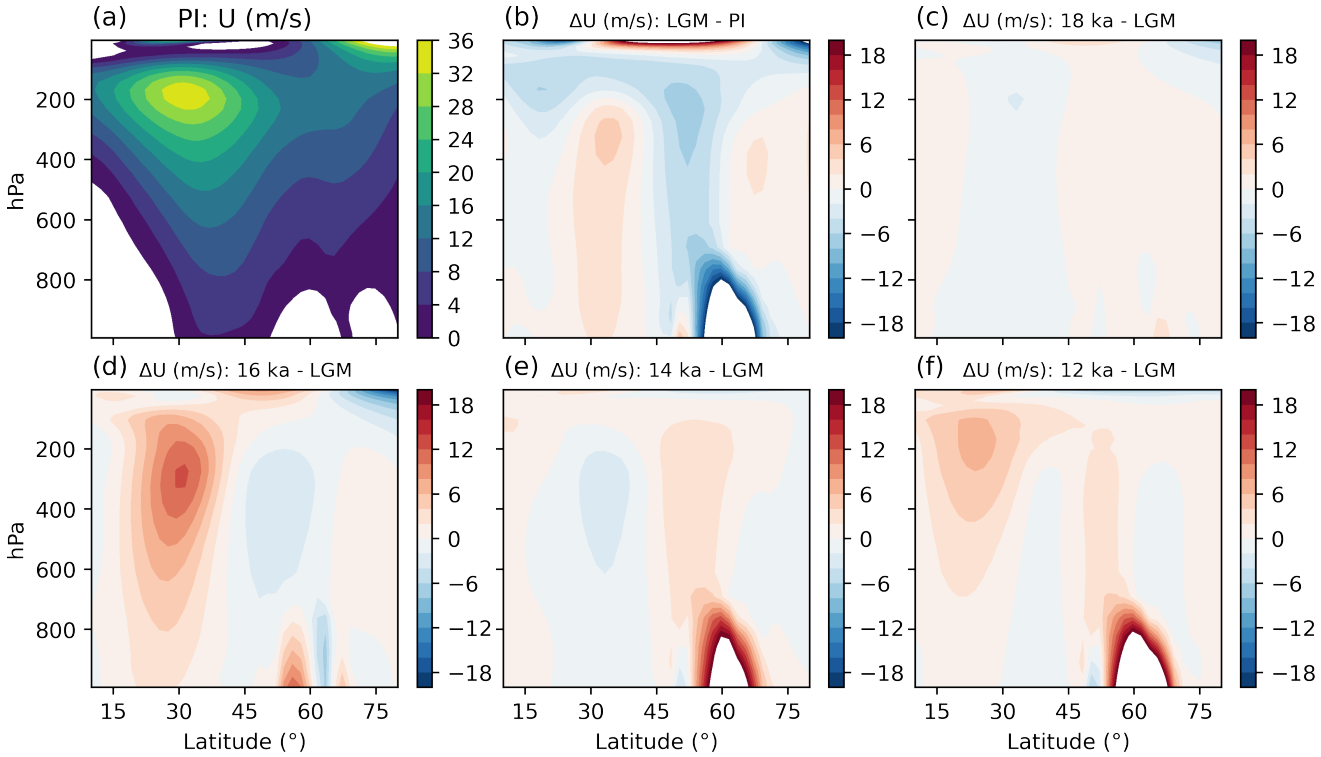

Figure S9. Winter-mean (DJF) zonal winds averaged over the eastern North Pacific (120°W–150°W) in iTraCE. (a) U (m/s) in the preindustrial simulation. (b) Difference between and LGM and PI. (c) Difference between 18 ka and LGM. (d–f) As in (c), but differences from LGM for 16 ka, 14 ka, and 12 ka, respectively.

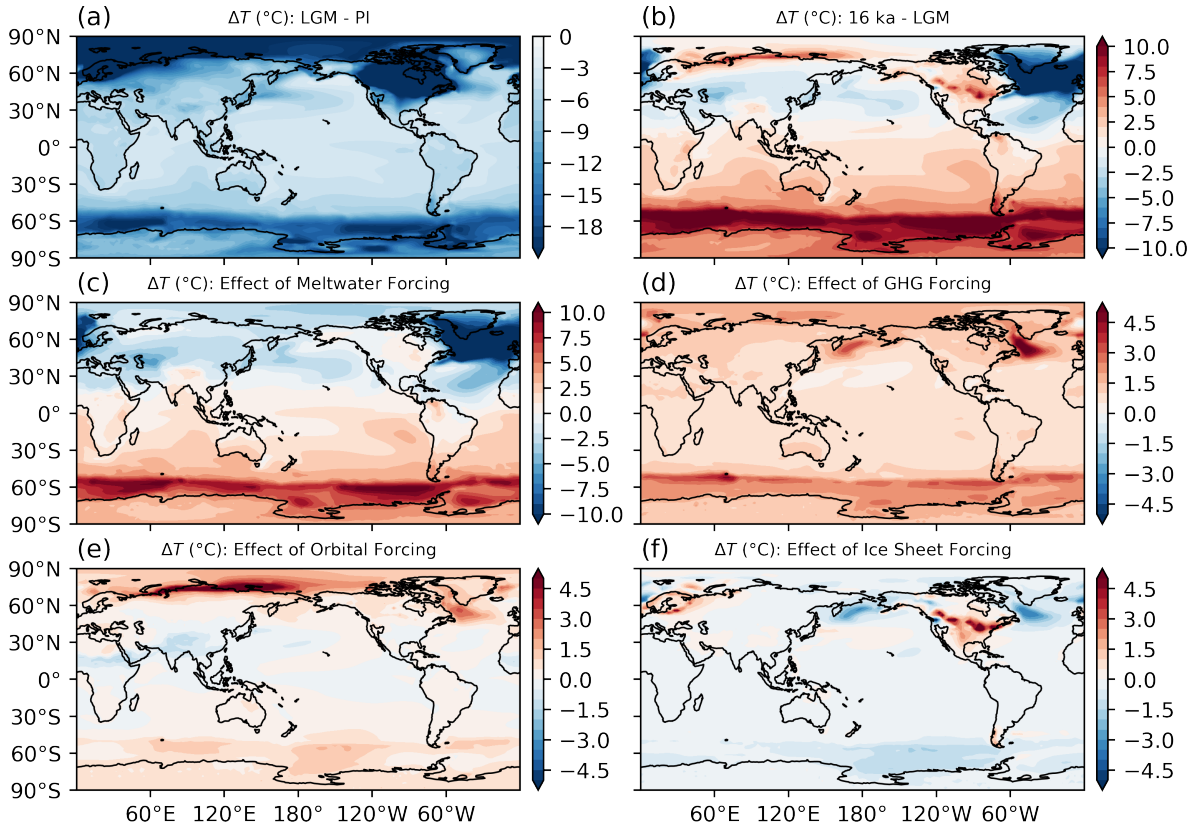

Figure S10. (a) Annual-mean surface temperature differences between LGM and PI in iTraCE. (b) Difference between 16 ka and LGM. (c) Difference in surface temperature from meltwater forcing (16 ka - 16 ka_ICE+ORB+GHG). (d) Difference from greenhouse gas forcing (16 ka_ICE+ORB+GHG - 16 ka_ICE+ORB). (e) Difference from insolation forcing (16 ka_ICE+ORB - 16 ka_ICE). (f) Difference from changing ice sheets and bathymetry (16 ka_ICE - LGM).

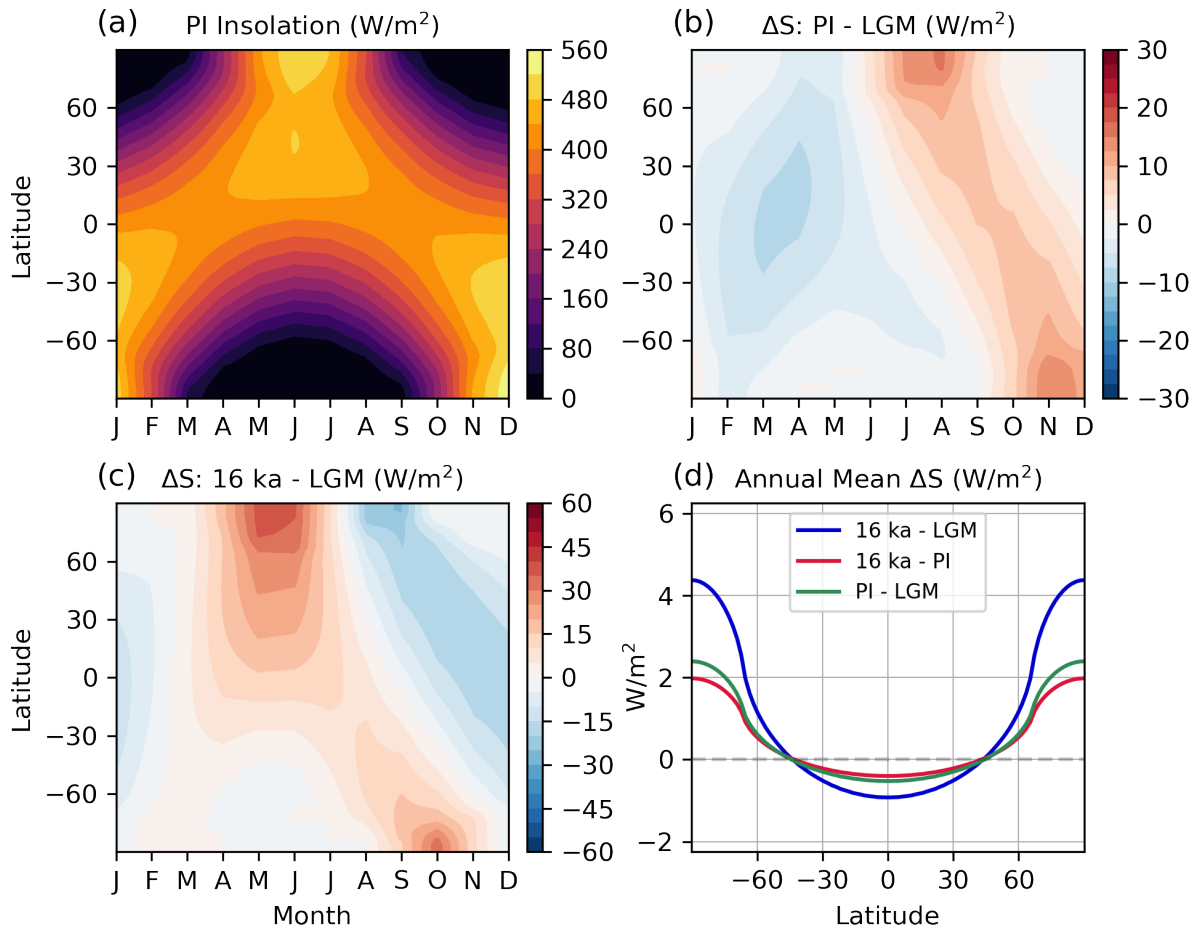

Figure S11. (a) Insolation as a function of season and latitude in the preindustrial simulation. (b) Difference in insolation between PI and LGM. (c) As in (b), but for the difference between 16 ka and LGM. (d) Zonal-mean insolation differences between 16 ka and LGM, 16 ka and PI, and PI and LGM, reflecting differences in obliquity. Vernal equinox is defined as March 21st at noon for all experiments.

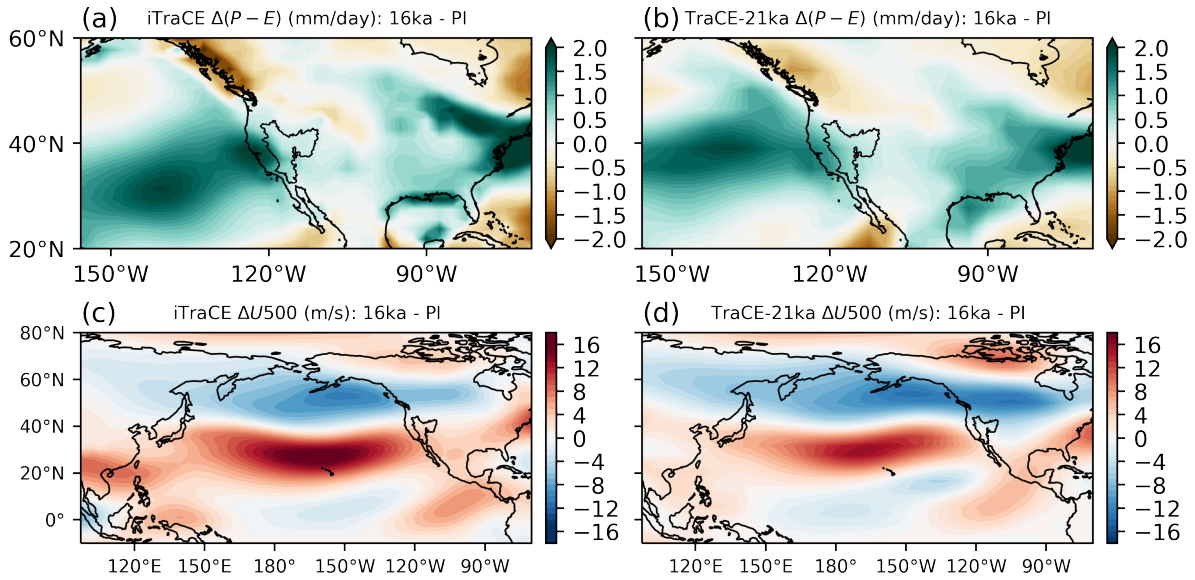

Figure S12. Difference in $(P - E)$ and North Pacific atmospheric circulation between 16 ka and PI. (a) Difference in $(P - E)$ between 16 ka and PI for iTraCE. (b) as in (a), but for TraCE-21ka. (c) Difference in winter-mean (DJF) zonal velocity at 500 hPa (U500; m/s) between 16 ka and PI for iTraCE. (d) as (c), but for TraCE-21ka.

References

Lüthi, D., Le Floch, M., Bereiter, B., Blunier, T., Barnola, J.-M., Siegenthaler, U., ... others (2008). High-resolution carbon dioxide concentration record 650,000–800,000 years before present. *nature*, *453*(7193), 379–382.

Monnin, E., Indermuhle, A., Dallenbach, A., Fluckiger, J., Stauffer, B., Stocker, T. F., ... Barnola, J.-M. (2001). Atmospheric CO_2 concentrations over the last glacial termination. *science*, *291*(5501), 112–114.

Peltier, W. R., Argus, D., & Drummond, R. (2015). Space geodesy constrains ice age terminal deglaciation: The global ice-6g_c (vm5a) model. *Journal of Geophysical Research: Solid Earth*, *120*(1), 450–487.